


Communication

A Coordination-Driven Self-Assembly and NIR Photothermal Conversion Study of Organometallic Handcuffs

Xiaoyan Lu ¹, Jing-Jing Huang ^{2,*}, Tian Chen ¹, Jie Zheng ^{1,3}, Ming Liu ¹, Xin-Yi Wang ¹, Yu-Xin Li ¹, Xinkai Niu ^{1,4} and Li-Long Dang ^{1,*}

¹ College of Chemistry and Chemical Engineering, Luoyang Normal University, Luoyang 471934, China

² Luoyang Institute of Science and Technology, Luoyang 471023, China

³ College of Materials and Chemical Engineering, China Three Gorges University, Yichang 443002, China

⁴ College of Science, Shihezi University, Shihezi 832003, China

* Correspondence: huangjingjingvip@163.com (J.-J.H.); danglilong8@163.com (L.-L.D.)

Abstract: Due to their fascinating topological structures and application prospects, coordination supramolecular complexes have continuously been studied by scientists. However, the controlled construction and property study of organometallic handcuffs remains a significant and challenging research subject in the area of supramolecular chemistry. Hence, a series of tetranuclear organometallic and heterometallic handcuffs bearing different size and metal types were rationally designed and successfully synthesized by utilizing a quadridentate pyridyl ligand (tetra-(3-pyridylphenyl)ethylene) based on three Cp^{*}Rh (Cp^{*} = η⁵-C₅Me₅) fragments bearing specific longitudinal dimensions and conjugated planes. These results were determined with single-crystal X-ray diffraction analysis technology, ESI-MS NMR spectroscopy, etc. Importantly, the photoquenching effect of Cp^{*} groups and the discrepancy of intermolecular π–π stacking interactions between building block and half-sandwich fragments promote markedly different photothermal conversion results. These results will further push the synthesis of topological structures and the development of photothermal conversion materials.

Keywords: coordination-driven self-assembly; half-sandwich fragment; organometallic handcuffs; photothermal conversion



Citation: Lu, X.; Huang, J.-J.; Chen, T.; Zheng, J.; Liu, M.; Wang, X.-Y.; Li, Y.-X.; Niu, X.; Dang, L.-L. A

Coordination-Driven Self-Assembly and NIR Photothermal Conversion Study of Organometallic Handcuffs. *Molecules* **2023**, *28*, 6826. <https://doi.org/10.3390/molecules28196826>

Academic Editor: Jiong Zhou

Received: 26 August 2023

Revised: 18 September 2023

Accepted: 26 September 2023

Published: 27 September 2023



Copyright: © 2023 by the authors. Licensee MDPI, Basel, Switzerland. This article is an open access article distributed under the terms and conditions of the Creative Commons Attribution (CC BY) license (<https://creativecommons.org/licenses/by/4.0/>).

1. Introduction

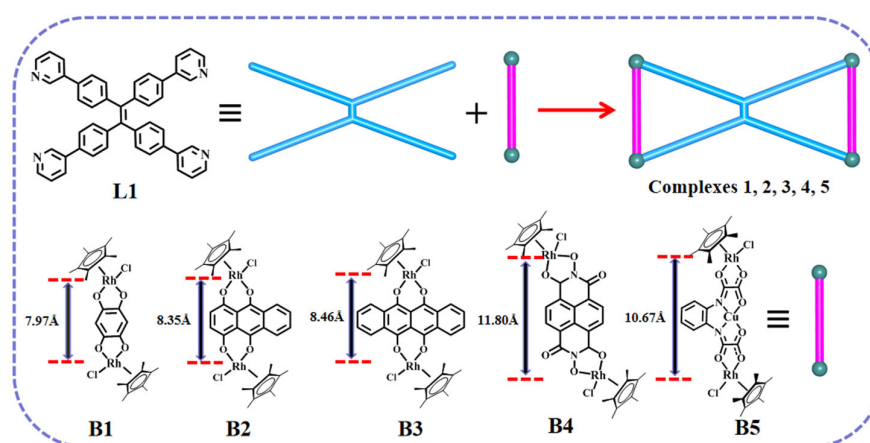
In recent decades, coordination supramolecular chemistry has made rapid progress and has become an important chemical field not only due to its exquisite topological structures but also for its dependence on promising application prospects in covering host–guest chemistry [1–4], biosimulation [5–7], fluorescence [8–10], photothermal response [11–13], etc. In the synthesis process of these complexes, the type of structure changes dramatically from simple to complicated topologies or from low to high order winding. After the efforts of previous scientists, the synthesis of initial macrocyclic compounds has evolved from [2] catenane compounds to Solomon, Borromean ring and [5] catenane structures, which have been well demonstrated by Sauvage, Stoddart, Fujita and Jin, etc. [14–23], marking the rapid development of the research field. At the same time, molecular knots and ravel have also experienced a rapid forward process. Studies from the original synthesis of trefoil knots have evolved to the construction of intricate knots and ravels in more than five crossings, including a pentafoil knot; +3₁ #+3₁ #+3₁ composite knot; granny knot and 8₁₈, 5₂, 7₁, and 9₁ knots [24–29]. These results pushed synthetic chemistry to a more sophisticated level. In addition, some non-intercable ring-in-ring structures and Russian doll assemblies are also continuously constructed to fill the scope of these exquisite topologies. Accompanied by the pursuit of the synthesis of these structures, structural transformations were explored by guest-, solvent- and metal ion-induced effects plus some chemical reactivity, etc., making it possible to synthesize some difficult compounds.

Scientists are also examining the properties of and applications for these complicated compounds. Some studies of organometallic macrocycle [30–33], cage [34–36], catenanes on luminescence [37–39], host–guest chemistry [40–42], separation [43–45], chiral resolution and catalysis [46–48] have made good progress. Professor Han proposed a new strategy to synthesize various carbonyl macrocyclic compounds and acquired some [2+2] cycloaddition organic products [49–51]. Zhang group synthesized a series of Pt^{2+} and Pd^{2+} based metal–organic cage compounds and investigated their aggregation-induced luminescence properties [38,39]. All these studies have played a great role in promoting research in this field.

Among the compounds constructed, a synthesis and property study of molecular handcuff compounds have been less explored due to the spatial effect of the interior structure, which makes the design difficult. Therefore, achieving synthesis and performing the property study of molecular handcuffs is significantly challenging.

Half-sandwich fragments have shown obvious advantages in the synthesis of supramolecular compounds due to their good solubility, crystallinity and directional coordination features. A series of specific supramolecular structures have been successfully synthesized, such as Borromean rings, Solomon links, [2–5] catenanes, 4-ravel and various knots [12,15,17–19,21,31]. Therefore, choosing appropriate organic linkers and half-sandwich building blocks with specific sizes might enable the construction of molecular handcuffs. In addition, the fluorescence quenching effect of half-sandwich fragments and the different intermolecular π – π stacking interactions possibly induce strong photothermal conversion properties.

L1, a tetradentate pyridine ligand, was chosen. In it, the central olefinic bond unit can keep 4 pyridine units in the same plane and generates a particular twist. The characteristics of a 3-pyridine unit could facilitate the coordination of 2 pyridine sites in the same ligand with half-sandwich metal ions, providing the conditions for the formation of molecular handcuffs. Here, a series of organometallic molecular handcuffs based on **B1–B5** building blocks bearing different lateral width and longitudinal dimensions were successfully constructed (Scheme 1). Structures were clearly confirmed by single crystal X-ray diffraction and NMR spectra. Additionally, photothermal conversion experiments have shown that these structures have different photothermal conversion properties due to differences in the size and conjugation effect of the building blocks **B1**, **B2**, **B3** and **B4**. Compound **4** exhibited a remarkable photothermal conversion performance.



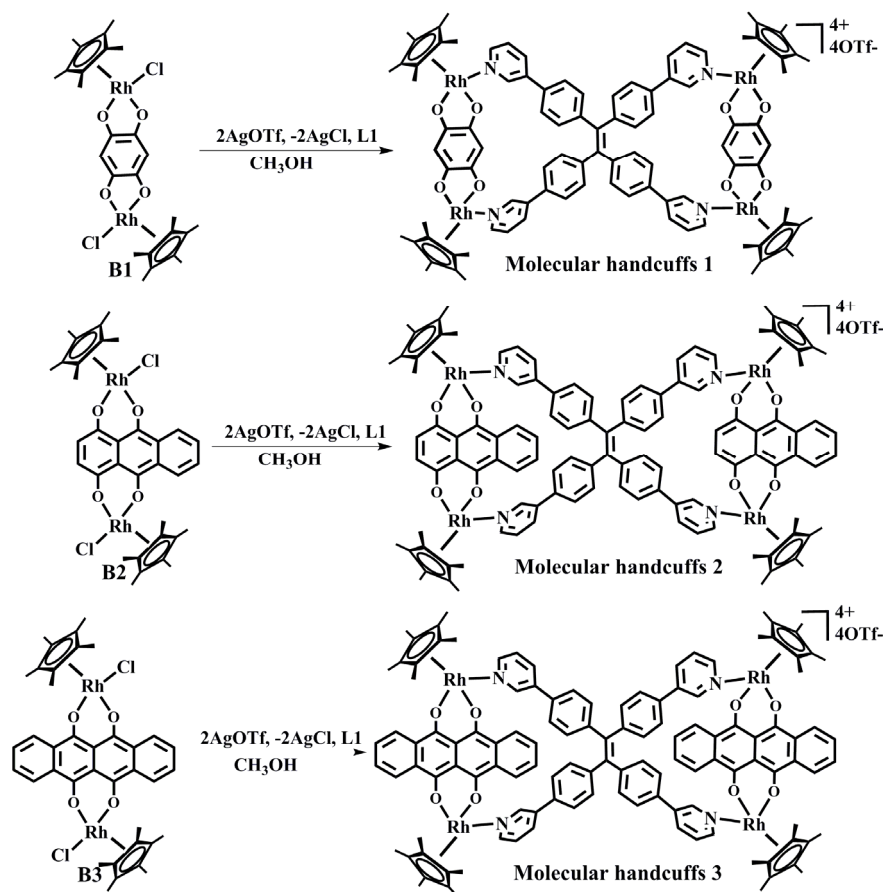
Scheme 1. The designed ligand **L1** and building blocks **B1**, **B2**, **B3**, **B4** and **B5**.

2. Results and Discussion

2.1. The Synthesis of Organometallic Handcuffs 1, 2, 3

The organic ligand **L1** and the three binuclear complexes **B1**, **B2** and **B3** were synthesized based on a previously reported method in the literature. The molecular handcuffs **1**, **2** and **3** were obtained by the reactions between ligand **L1** and **B1**, **B2** or **B3**, as shown in Scheme 2. **B1**, **B2** or **B3** was first reacted with two equivalents of silver trifluoromethane-

sulfonate (AgOTf) under dark conditions. Then, silver chloride was removed through centrifugation so that rhodium salt could be connected to the bridging donor ligand **L1**. Subsequently, the **L1** ligand was added into the solution above, and products **1**, **2** and **3** were extracted with methanol/isopropyl ether with yields of 85.7%, 84.8% and 83.4%, respectively. At room temperature, isopropyl ether was slowly diffused into a solution of complex **1** in methanol, and over a period of two days, single crystals of complex **1** were obtained.



Scheme 2. The synthesis of molecular handcuff compounds (**1**, **2** and **3**).

2.2. The Self-Assembly and Structural Analysis of Molecular Handcuffs **1**

Single-crystal X-ray analysis and an NMR spectrum confirmed the structure of complexes **1** as shown in Figure 1. The two Rh^{III} molecular clips in **B1** are linked to four pyridyl sites of one ligand **L1**, generating two rings connected by a central olefinic bond, forming a very interesting handcuffed complex **1**, which exhibits short and long Rh–Rh nonbonding distances of 7.97 and 17.35 Å. Viewed from the side, the two molecular clips **E1** are placed in a trans configuration, generating a Z-shaped structure. Furthermore, the stacking pattern analysis revealed no interactions between the molecules, suggesting that individual discrete molecules can be stable.

Additionally, the presence of molecular handcuffs **1** under solution conditions were also demonstrated by the ¹H NMR spectrum (Figure 2), accompanied by the combination of ¹H–¹H COSY NMR and ¹H–¹H DOSY NMR spectra (Figure 3a,b). Two obvious coupled double peaks could be observed at 8.64 and 8.11 ppm in complex **1**, and it displayed an obvious coupling interaction with the triplet at 7.58 ppm, which belonged to the a, b, c positions of the meta-position pyridine group of **L1**. Two phenyl proton signals—e, f—could be found at 7.35, 7.21 ppm and 8.68 ppm. Additionally, two strong singlets in the aromatic region could be found at 8.68 and 8.57 ppm, which belonged to the pyridyl proton and benzoquinone proton building block **E1**. In addition, the signal of Cp* group was

at 1.82 ppm (Figure 2). The ^1H DOSY NMR spectrum of **1** demonstrated that signals for the aromatic and Cp* units displayed a single diffusion coefficient ($2.74 \times 10^{-6} \text{ cm}^2 \text{ s}^{-1}$), further determining the stable presence of **1** (Figure 3b). In addition to NMR spectroscopic data, the presence of complex **1** was also determined by ESI-MS: $[\text{1-2OTf}]^{2+}$ ($m/z = 1083.12$) and $[\text{1-3OTf}]^{3+}$ ($m/z = 672.43$) (Figure 4).

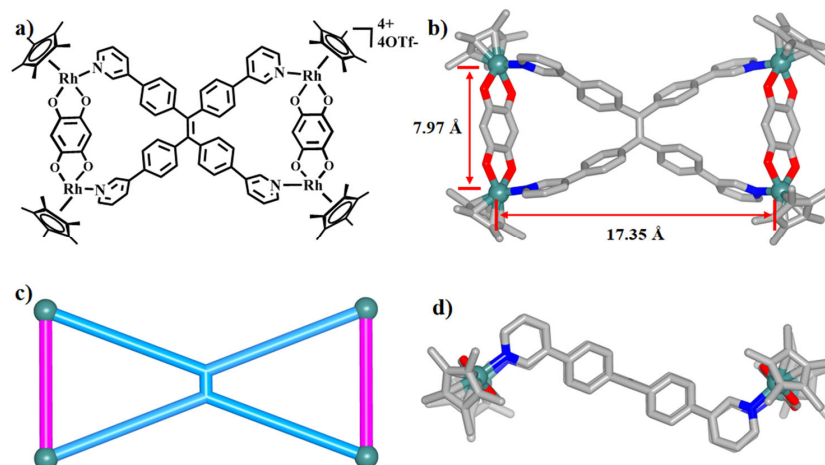


Figure 1. (a) The chemical structure of molecular handcuffs **1**; (b) the solid-state structure of **1**, showing the Rh–Rh nonbonding distances; (c) a simplified topological representation of the structure of **1**; (d) a top view of the structure of **1**. All hydrogen atoms were omitted for clarity (N, blue; C, gray; Rh, Aqua; Cl, green).

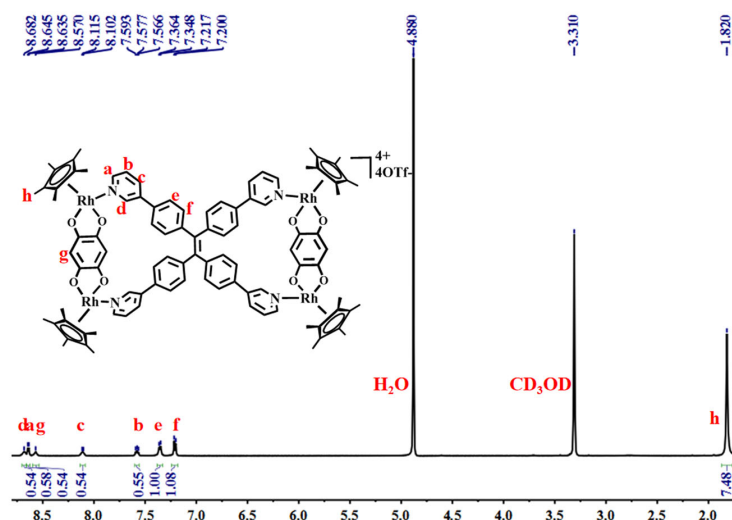


Figure 2. The ^1H NMR (500 MHz, CD_3OD , ppm) for **1** (7.0 mM, with respect to Cp^*Rh).

2.3. The Self-Assembly and Structural Analysis of Molecular Handcuffs **2** and **3**

The molecular handcuff structure **1** prompts us to explore whether increasing the width of a Cp*–based building block can induce the difference in topological structure. Therefore, building blocks **B2** and **B3** were individually introduced into the system to carry out a reaction with ligand **L1**. Once the two reaction processes were completed, the NMR exploration experiments of complexes **2** and **3** were performed. The ^1H NMR of complex **1** exhibited a clear set of proton signals (Figure 5), which were analyzed through the combination with the two-dimensional spectra of ^1H – ^1H COSY NMR and ^1H – ^1H DOSY NMR (Figure 6a,b). Two doublet signals at 8.68 ppm and 8.05 ppm were clearly observed, which had an obvious coupling effect with the same triplet at 7.57 ppm. Thus, the three signals belonged to the pyridinyl protons of ligand **L1**. A pair of coupled doublets at 7.01 ppm and a singlet in 6.90 ppm were due to the pyridinyl and phenyl protons of **L1**.

In addition, a doublet at 7.26 ppm without coupling with other protons and two coupling multiple peaks at 8.73 and 8.02 ppm were due to the phenyl protons of the E2 building units. The chemical shift of the Cp* proton was at 1.73 ppm. A single diffusion coefficient from the ^1H - ^1H DOSY NMR spectrum ($2.88 \times 10^{-6} \text{ cm}^2\text{s}^{-1}$) further demonstrated the presence of complex 2 (Figure 6b). Likewise, the ^1H NMR of complex 3 was analyzed, also showing a set of simple and clear proton signals. Most proton conditions were similar to those in compounds 1 and 2, demonstrating the formation of molecular handcuffs 3 (Figures 1–3). This study showed that increasing the width did not change the structural types of molecular handcuffs.

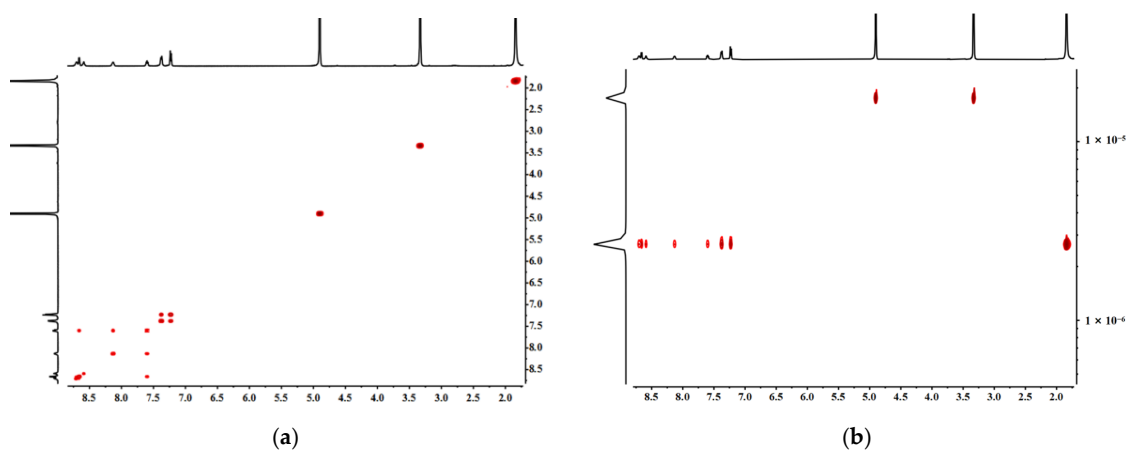


Figure 3. (a) The ^1H - ^1H COSY NMR (500 MHz, CD_3OD , ppm) for 1; (b) The ^1H - ^1H DOSY NMR (500 MHz, CD_3OD , ppm) for 1 ($2.74 \times 10^{-6} \text{ cm}^2\text{s}^{-1}$) (7.0 mM, with respect to Cp^*Rh).

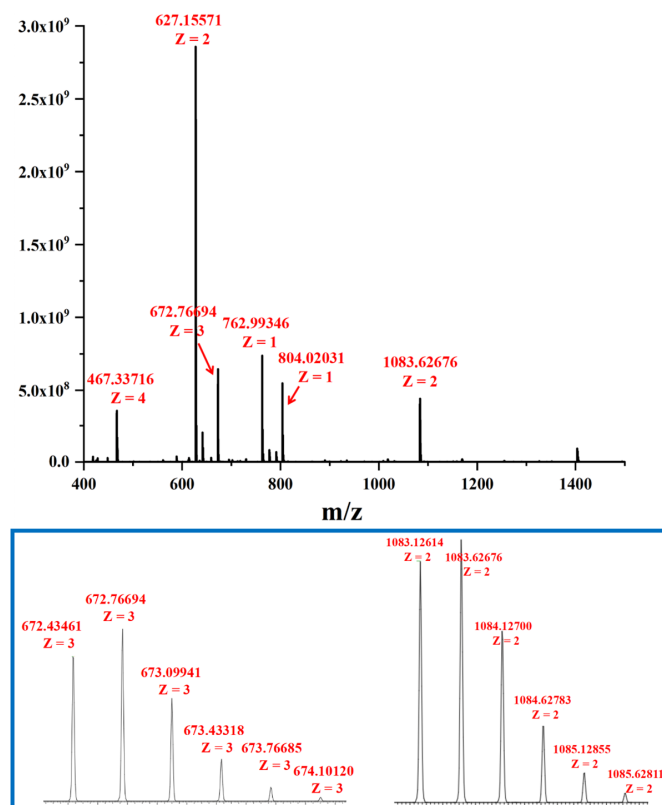


Figure 4. The full ESI-TOF-MS spectrum of complex 1; 2^+ and 3^+ mass peaks of 1.

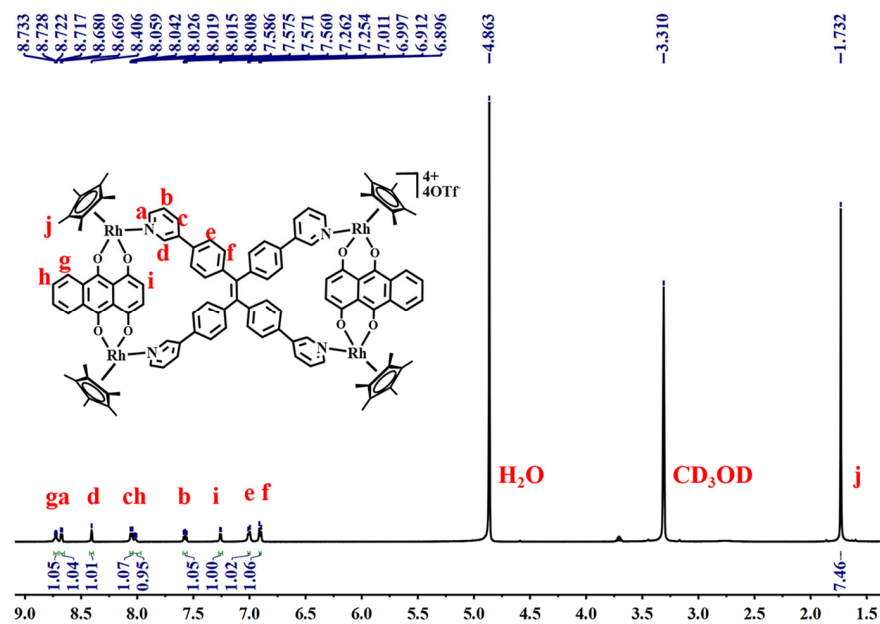


Figure 5. The ^1H NMR (500 MHz, CD_3OD , ppm) for **2** (12.0 mM, with respect to Cp^*Rh).

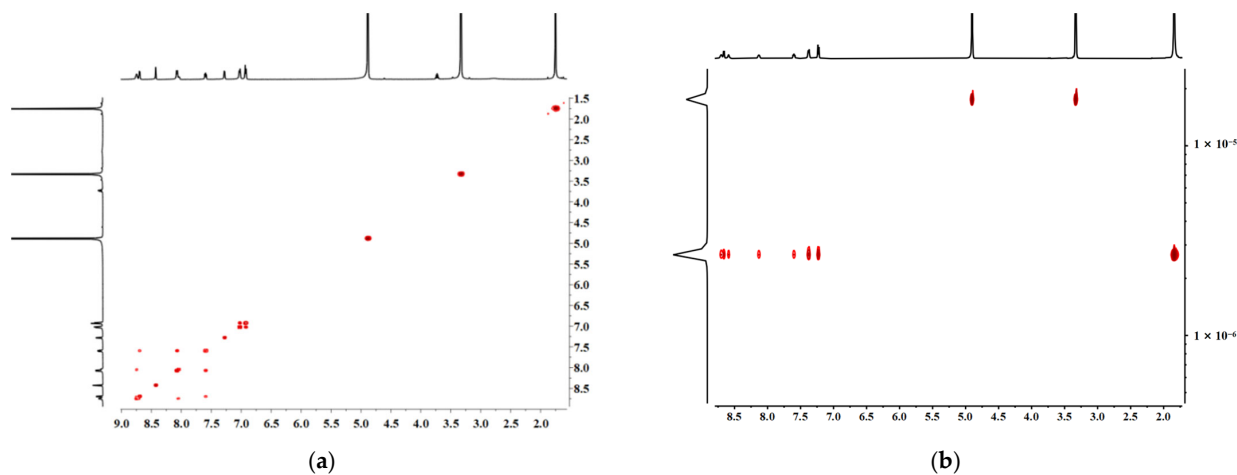
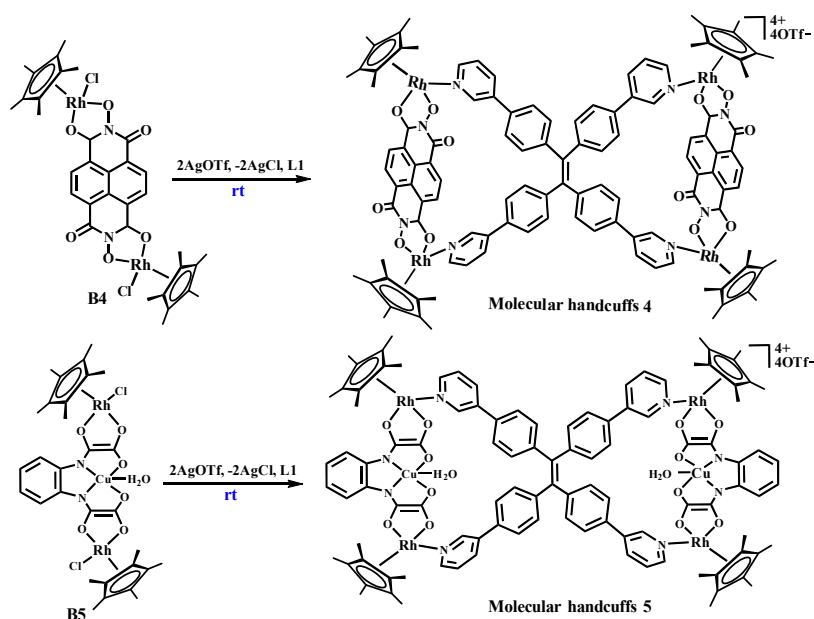


Figure 6. (a) The ^1H - ^1H COSY NMR (500 MHz, CD_3OD , ppm) for **2** and (b) the ^1H - ^1H DOSY NMR (500 MHz, CD_3OD , ppm) for **2** ($2.88 \times 10^{-6} \text{ cm}^2\text{s}^{-1}$) (12.0 mM, with respect to Cp^*Rh).

2.4. The Self-Assembly of Molecular Handcuffs **4** and Heterometallic Handcuffs **5**

Next, to explore the effect of the size of the building blocks on the structural synthesis, two longer building blocks **B4** and a heterometallic $[\text{Cp}^*_2\text{Rh}_2\text{L}^{\text{Cu}}]\text{Cl}_2$ ($\text{L}^{\text{Cu}} = [\text{Cu}(\text{opba})]^{2-}$ [opba = o-phenylenebis(oxamato)]) (**B5**) were deliberately selected to synthesize a bigger organometallic assembly, in which the Rh–Rh nonbonding distances were 11.80 and 10.67 Å. Through the self-assembly of ligand **L1** and building blocks **B4** and **B5**, two new gray and green centrosymmetric complexes **4** and **5** were obtained in the yields of 85.8% and 83.6% (Scheme 3). Despite various attempts, we did not obtain a single crystal structure of complex **4**. Fortunately, the structure of complex **5** was ensured by single crystal X-ray diffraction.



Scheme 3. The synthesis of handcuffs **4** and heterometallic handcuffs **5**.

Complex **4** was dissolved in deuterated methanol to explore its solution behavior. The ^1H NMR of complex **4** displayed a set of clear proton signals (Figure 7), which were determined by the utilization of the two-dimensional spectra of ^1H - ^1H COSY NMR and ^1H - ^1H DOSY NMR (Figure 8a,b). A triplet at 7.59 ppm has obvious coupling interactions with two doublets at 8.65 and 8.10 ppm, which is consistent with the three adjacent proton environments of the meta-position pyridine group of **L1**; these protons could be attributed to the a, b, c positions of the pyridine unit. In addition, two doublets at 7.34 and 7.22 ppm with coupling interactions belonged to e, f of the phenyl unit. Additionally, two strong singlets in the aromatic region could be found at 8.68 and 8.57 ppm. Furthermore, the signals of the NDI unit and Cp* group in building block **B4** could be located at 8.88 and 1.82 ppm (Figure 6). The ^1H DOSY NMR spectrum of **4** obviously exhibited that these signals for the aromatic and Cp* units displayed a single diffusion coefficient ($2.34 \times 10^{-6} \text{ cm}^2 \text{ s}^{-1}$), further determining the stable presence of **4** (Figure 8b).

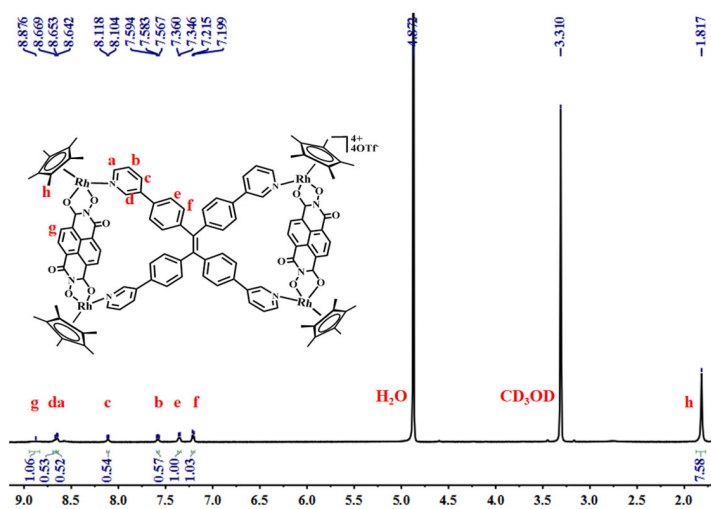


Figure 7. The ^1H NMR (500 MHz, CD_3OD , ppm) for **2** (7.0 mM, with respect to Cp^*Rh).

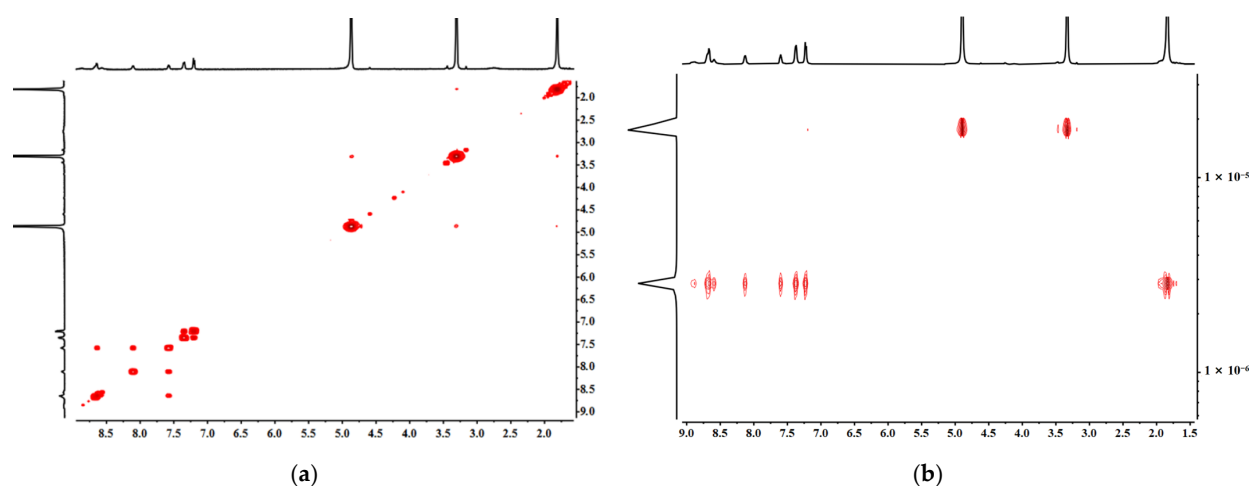


Figure 8. (a) The ^1H - ^1H COSY NMR (500 MHz, CD_3OD , ppm) for **4** and (b) the ^1H - ^1H DOSY NMR (500 MHz, CD_3OD , ppm) for **4** ($2.34 \times 10^{-6} \text{ cm}^2\text{s}^{-1}$) (7.0 mM, with respect to Cp^*Rh).

Moreover, single crystals suitable for X-ray structure determination were obtained via slow vapor diffusion of isopropyl ether into a methanol solution of **5** at room temperature, displaying the acquisition of interesting heterometallic handcuffs, which included two metal ions, rhodium ions and copper ions. The single crystal structure showed that the distance between the two Rh–Rh that were coordinated with the pyridinyl group was about 11.80 and 10.67 Å, respectively. The longest distance of Rh–Rh was 16.17 Å, which is similar to the distances of complexes **1** and **2**. Careful observation revealed that an obvious accumulation effect (3.48 Å) between Cp^* and the phenyl group could be observed, reflecting strong intermolecular interactions. These interactions caused the formation of two-dimensional layered structures. (Figure 9).

2.5. Photothermal Conversion Studies

Photothermal materials are widely used in the fields of photothermal therapy, photothermal imaging and photothermal sensors [52,53]. Previous research showed that half-sandwich structures have a very strong light quenching effect. The dark appearance and near infrared absorption of these half-sandwich-based molecular handcuffs prompted us to investigate their photothermal conversion performance, which have also attracted more and more attention of scientists [54]. First, the solid UV-visible spectra of complexes **1**, **2**, **3**, **4** and **5** were recorded (Figure 10a). Results showed a set of obvious near infrared absorption: 0.84, 0.70, 0.74, 1.0 and 0.22 at 730 nm for complexes **1**, **2**, **3**, **4** and **5**, respectively. Analyzing these absorption values carefully, we could find that complexes **4** and **5** showed the strongest and weakest near infrared absorption, which are related to their conjugation effect and copper ion coordination characteristics. This might have resulted in the strongest and weakest photothermal conversion effect. Meanwhile, a similar absorption value of complexes **1**, **2**, **3** could be attributed to their close conjugation effect. These near infrared absorption values could generate a corresponding NIR photothermal conversion ability.

Subsequently, the NIR photothermal conversion studies for complexes **1**, **2**, **3**, **4** and **5** were separately carried out. And the photothermal conversion curves of these complexes showed a specific heating process. The temperature of complex **1** under 0.6 W/cm^2 laser irradiation at a 730 nm wavelength displayed a significant increase at $9.5 \text{ }^\circ\text{C}$ (from 26.7 to $36.2 \text{ }^\circ\text{C}$, Figure 10b). Meanwhile, the observed temperature changes for complexes **2** (from 27.4 to $43.6 \text{ }^\circ\text{C}$) and **3** (from 27.4 to $35.8 \text{ }^\circ\text{C}$) are similar to that recorded for complex **1**. Importantly, an obvious stronger photothermal conversion could be observed for molecular handcuffs **4**. Thus, a temperature increase of $26.7 \text{ }^\circ\text{C}$ (from 27.7 to $54.4 \text{ }^\circ\text{C}$) in 230 s under a power irradiation (0.15 W/cm^2 , Figure 10b), which could be due to the suitable conjugation effect of building block **B4**, resulted in the strongest near infrared (NIR) absorption (1.0) at

730 nm and intermolecular π - π stacking interactions, leading to a good NIR photothermal conversion effect. Nevertheless, just as we expected, the weak near infrared absorption (0.22) at 730 nm and poor intermolecular π - π stacking interactions in complex 5 resulted in a very small temperature change of about 6.4 °C (from 26.2 °C to 32.4 °C), which was consistent with our initial speculation.

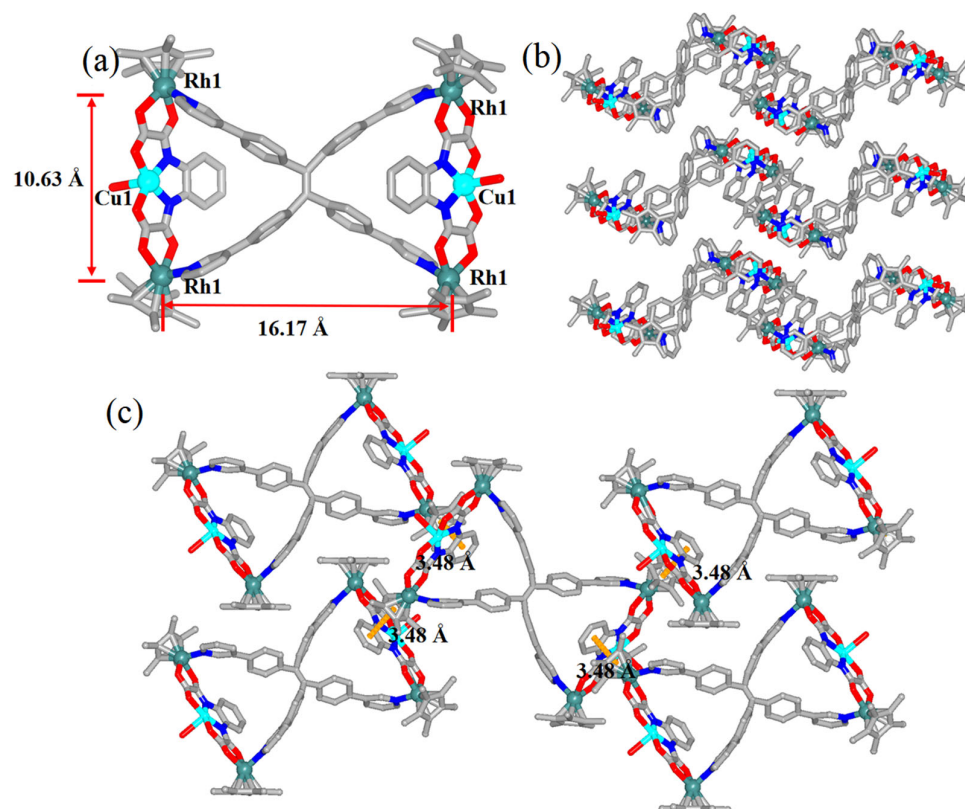


Figure 9. (a) The molecular structure of heterometallic handcuffs 5. (b) A side view of heterometallic handcuffs 4. (c) A top view of heterometallic handcuffs 4 (π - π stacking interactions: 3.48 Å). OTf⁻ and solvent molecules outside the framework and hydrogen atoms are omitted (O, red; N, blue; C, gray; H, pink; Rh, Aqua; Cu, cyan).

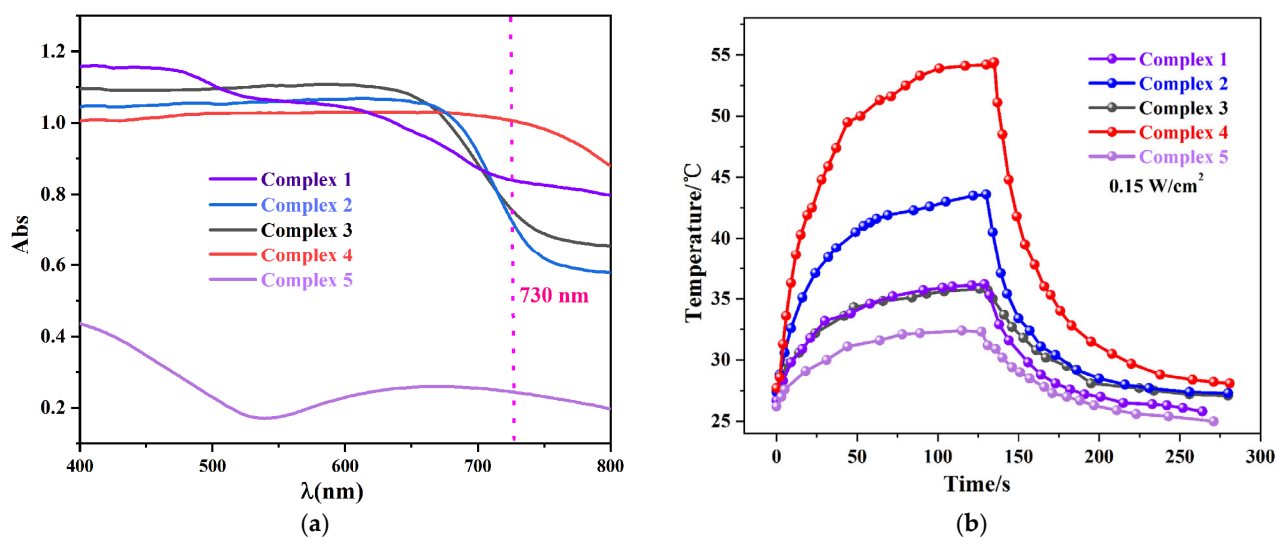


Figure 10. (a) The UV-Vis absorption spectrum of complexes 1, 2, 3, 4 and 5 (400–800 nm); and (b) the NIR photothermal conversion curves of metallarectangles 1, 2, 3, 4 and 5.

Due to the excellent photothermal conversion performance of complex 4 at the laser power per unit area of 0.15 W/cm^2 at 730 nm , we continued to study the photothermal conversion ability under different laser power per unit areas: $0.15, 0.3, 0.45 \text{ W/cm}^2$ at 730 nm (Figure 11a). Results showed that accompanied by the increase in laser power per unit area from 0.15 to 0.45 W/cm^2 , temperature change increased accordingly (Figure 11b). Specifically, when the power per unit area was 0.45 W/cm^2 , the temperature change of complex 4 could reach $55.7 \text{ }^\circ\text{C}$ (from $28.7 \text{ }^\circ\text{C}$ to $84.4 \text{ }^\circ\text{C}$), suggesting that in a special near infrared light region, the increase in laser power per unit area could result in the enhancing of the photothermal conversion performance.

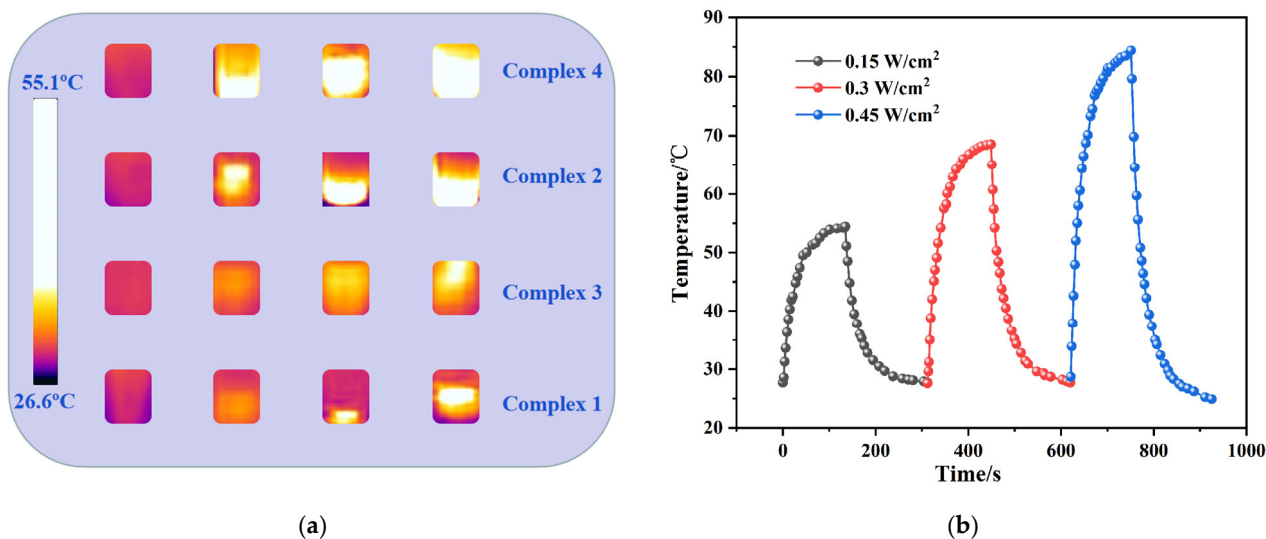


Figure 11. (a) NIR thermal images of metallarectangles 1, 2, 3, and 4 in the spectrophotometer cell ($1 \times 1 \times 5 \text{ cm}$) under 730 nm laser irradiation and (b) NIR photothermal conversion curves of 4 under $0.15, 0.3, 0.45 \text{ W/cm}^2$ laser irradiation at 730 nm .

3. Experiment

Materials

All reagents and solvents were commercially purchased and used without further purification. The starting materials **B1**, **B2**, **B3**, **B4** and $[\text{Cp}^*\text{Rh}_2(\text{L}^{\text{Cu}})]\text{Cl}_2$ (**B5**) were synthesized based on a previously reported method in the literature. NMR spectra were taken at room temperature using Bruker AVANCE I 500 spectrometers. Elemental analyses were collected on an Elementar Vario EL III analyzer.

4. Conclusions

In summary, a series of organometallic molecular handcuffs bearing different sizes and species of metal atoms were successfully acquired through the self-assembly of quadri-dentate pyridyl ligand **L1** and the five Cp^*Rh based building blocks **B1**, **B2**, **B3**, **B4** and **B5**. The change of the width and length of building blocks did not cause the change of the type of molecular handcuffs. And, these complexes were characterized by single crystal X-ray diffraction analysis, NMR spectra and UV–Vis spectra. Interestingly, the photothermal conversion studies for these complexes are carefully performed, reflecting different photothermal conversion capacities. Discrepancy in photothermal conversion comes from the different conjugative effects of building blocks **B1–B5**. A strong conjugation effect and π – π stacking interactions induced good photothermal conversion results. We believe that our results may be useful for constructing various Cp^* -based photothermal conversion materials and promoting the rapid development of fine materials and smart materials.

Author Contributions: X.L. and J.-J.H.: synthesis of the title complexes, formal analysis. T.C. and Y.-X.L.: IR-related experiment. J.Z. and M.L.: completed formal analysis and NMR tests. X.-Y.W. and X.N.: completed UV-Vis spectra experiment. L.-L.D.: Supervision, writing—review and editing. All authors have read and agreed to the published version of the manuscript.

Funding: This work was supported by the National Natural Science Foundation of China (Grant Nos. 22101108 and 22102068), Natural Science Foundation of Henan Province (No. 212300410209), the Shanghai Science Technology Committee (19DZ2270100), the Natural Science Foundation for Excellent Young Scholars of Henan Province (232300421083), Key Scientific Research Projects of Higher Education of He'nan Province (22A150016) and the Heluo Young Talent Lifting Project (2022HLTJZC09 and 2023HLTJ02).

Institutional Review Board Statement: Not applicable.

Informed Consent Statement: Not applicable.

Data Availability Statement: Not applicable.

Conflicts of Interest: The authors declare no conflict of interest.

References

1. Percástegui, E.G.; Ronson, T.K.; Nitschke, J.R. Design and applications of Water-Soluble coordination cages. *Chem. Rev.* **2020**, *120*, 13480–13544. [[CrossRef](#)]
2. Northrop, B.H.; Zheng, Y.R.; Chi, K.W.; Stang, P.J. Self-Organization in Coordination-Driven Self-Assembly. *Acc. Chem. Res.* **2009**, *42*, 1554–1563. [[CrossRef](#)]
3. Clever, G.H.; Punt, P. Cation–Anion arrangement patterns in Self-Assembled Pd₂L₄ and Pd₄L₈ coordination cages. *Acc. Chem. Res.* **2017**, *50*, 2233–2243. [[CrossRef](#)]
4. Ibáñez, S.; Poyatos, M.; Peris, E. N-Heterocyclic carbenes: A door open to supramolecular organometallic chemistry. *Acc. Chem. Res.* **2020**, *53*, 1401–1413. [[CrossRef](#)]
5. Zhou, Z.; Wang, Y.; Peng, F.; Meng, F.; Zha, J.J.; Ma, L.; Du, Y.H.; Peng, N.; Ma, L.F.; Zhang, Q.H.; et al. Intercalation-activated layered MoO₃ nanobelts as biodegradable nanozymes for tumor-specific photo-enhanced catalytic therapy. *Angew. Chem. Int. Ed.* **2022**, *61*, e202115939. [[CrossRef](#)]
6. Pöthig, A.; Casini, A. Recent developments of supramolecular Metal-based structures for applications in cancer therapy and imaging. *Theranostics* **2019**, *9*, 3150–3169. [[CrossRef](#)]
7. Shan, W.L.; Lin, Y.J.; Hahn, F.E.; Jin, G.X. Highly selective synthesis of Iridium(III) metalla [2]catenanes through component Pre-Orientation by $\pi \cdots \pi$ stacking. *Angew. Chem. Int. Ed.* **2019**, *58*, 5882–5886. [[CrossRef](#)]
8. Chakrabarty, R.; Mukherjee, P.S.; Stang, P.J. Supramolecular coordination: Self-Assembly of finite Two- and Three-Dimensional ensembles. *Chem. Rev.* **2011**, *111*, 6810–6918. [[CrossRef](#)]
9. Garci, A.; David, A.H.G.; Le Bras, L.; Ovalle, M.; Abid, S.; Young, R.M.; Liu, W.; Azad, C.S.; Brown, P.J.; Wasielewski, M.R.; et al. Thermally Controlled Exciplex Fluorescence in a Dynamic Homo[2]catenane. *J. Am. Chem. Soc.* **2022**, *144*, 23551–23559. [[CrossRef](#)]
10. Denis, M.; Goldup, S.M. A [3]Rotaxane host selects between stereoisomers. *Angew. Chem. Int. Ed.* **2018**, *57*, 4462–4464. [[CrossRef](#)]
11. Hu, S.J.; Guo, X.Q.; Zhou, L.P.; Yan, D.N.; Cheng, P.M.; Cai, L.X.; Li, X.Z.; Sun, Q.F. Guest-driven self-assembly and chiral induction of photofunctional lanthanide tetrahedral cages. *J. Am. Chem. Soc.* **2022**, *144*, 4244–4253. [[CrossRef](#)]
12. Dang, L.L.; Sun, Z.B.; Shan, W.L.; Lin, Y.J.; Li, Z.H.; Jin, G.X. Coordination-driven self-assembly of a molecular figure-eight knot and other topologically complex architectures. *Nat. Commun.* **2019**, *10*, 2057. [[CrossRef](#)]
13. Wang, H.; Qin, J.; Huang, C.; Han, Y.; Xu, W.; Hou, H. Mono/bimetallic water-stable lanthanide coordination polymers as luminescent probes for detecting cations, anions and organic solvent molecules. *Dalton Trans.* **2016**, *45*, 12710–12716. [[CrossRef](#)]
14. Forgan, R.S.; Sauvage, J.-P.; Stoddart, J.F. Chemical Topology: Complex Molecular Knots, Links, and Entanglements. *Chem. Rev.* **2011**, *111*, 5434–5464. [[CrossRef](#)]
15. Sauvage, J.-P. From Chemical Topology to Molecular Machines (Nobel Lecture). *Angew. Chem. Int. Ed.* **2017**, *56*, 11080–11093. [[CrossRef](#)]
16. Dang, L.L.; Li, T.T.; Zhang, T.T.; Zhao, Y.; Chen, T.; Gao, X.; Ma, L.F.; Jin, G.X. Highly selective synthesis and near-infrared photothermal conversion of metalla-Borromean ring and [2]catenane assemblies. *Chem. Sci.* **2022**, *13*, 5130–5140. [[CrossRef](#)]
17. Yi, X.; Zhang, H.-N.; Lin, Y.-J.; Jin, G.-X. Selective Construction of Molecular Borromean Rings And [2]catenane Utilizing Ether Bipyridyl Ligands. *Chem. Eur. J.* **2023**, *29*, e202204038. [[CrossRef](#)]
18. Zhou, M.-Y.; Yu, Z.-S.; Deng, W.; Lu, H.-L.; Niu, X.-F.; Tong, J.; Yu, S.-Y.; Fujita, M. [M₈L₄]⁸⁺-Type Squares Self-Assembled by Dipalladium Corners and Bridging Aromatic Dipyrzole Ligands for Iodine Capture. *Inorg. Chem.* **2023**, *62*, 10193–10202. [[CrossRef](#)]
19. Cui, Z.; Gao, X.; Lin, Y.-J.; Jin, G.-X. Stereoselective self-assembly of complex chiral radial [5]catenanes using half-sandwich rhodium/iridium building blocks. *J. Am. Chem. Soc.* **2022**, *144*, 2379–2386. [[CrossRef](#)]

20. Zou, Y.; Zhang, H.-N.; Mu, Q.-S.; Dang, L.-L.; Jin, G.-X. Selective Construction of Borromean Rings and Tweezer-Like Molecular Assembly Featuring Cp*Rh/Ir Clips for Near-Infrared Photothermal Conversion. *Chin. J. Chem.* **2023**, *41*, 3229–3237. [[CrossRef](#)]
21. Gao, W.X.; Feng, H.J.; Lin, Y.J.; Jin, G.X. Covalent Post-assembly modification triggers structural transformations of borromean rings. *J. Am. Chem. Soc.* **2019**, *141*, 9160–9164. [[CrossRef](#)]
22. Gao, W.X.; Feng, H.J.; Guo, B.B.; Lu, Y.; Jin, G.X. Coordination-Directed Construction of Molecular Links. *Chem. Rev.* **2020**, *120*, 6288–6325. [[CrossRef](#)]
23. Cui, Z.; Mu, Q.-S.; Gao, X.; Jin, G.-X. Stereoselective Construction of Chiral Linear [3]Catenanes and [2]Catenanes. *J. Am. Chem. Soc.* **2023**, *145*, 725–731. [[CrossRef](#)]
24. Zhang, L.; Stephens, A.J.; Lemonnier, J.F.; Pirvu, L.; Vitorica-Yrezabal, I.J.; Robinson, C.J.; Leigh, D.A. Coordination chemistry of a Molecular pentafoil knot. *J. Am. Chem. Soc.* **2019**, *141*, 3952–3958. [[CrossRef](#)]
25. Zhang, L.; Stephens, A.J.; Nussbaumer, A.L.; Lemonnier, J.F.; Jurcek, P.; Vitorica-Yrezabal, I.J.; Leigh, D.A. Stereoselective synthesis of a composite knot with nine crossings. *Nat. Chem.* **2018**, *10*, 1083–1088. [[CrossRef](#)]
26. Leigh, D.A.; Schaufelberger, F.; Piruv, L.; Stenlid, J.H.; August, D.P.; Segard, J. Tying different knots in a molecular strand. *Nature* **2020**, *584*, 562–568. [[CrossRef](#)]
27. Inomata, Y.; Sawada, T.; Fujita, M. Metal-Peptide Torus Knots from Flexible Short Peptides. *Chem* **2020**, *6*, 294–303. [[CrossRef](#)]
28. Leigh, D.A.; Danon, J.J.; Fielden, S.D.P.; Lemonnier, J.-F.; Whitehead, G.F.S.; Woltering, S.L. A molecular endless (7₄) knot. *Nat. Chem.* **2021**, *13*, 117–122. [[CrossRef](#)]
29. Dang, L.L.; Zhang, T.T.; Chen, T.; Zhao, Y.; Gao, X.; Francisco, A.; Ma, L.F.; Jin, G.X. Selective Synthesis and Structural Transformation of a 4-Ravel Containing Four Crossings and Featuring Cp*Rh/Ir Fragments. *Angew. Chem. Int. Ed.* **2023**, *62*, e202301516. [[CrossRef](#)]
30. Liu, X.-R.; Cui, P.-F.; Guo, S.-T.; Lin, Y.-J.; Jin, G.-X. “Cage Walking” Synthetic Strategy for Unusual Unsymmetrical Supramolecular Cages. *J. Am. Chem. Soc.* **2023**, *145*, 8569–8575. [[CrossRef](#)]
31. Lu, Y.; Liu, D.; Cui, Z.; Lin, Y.J.; Jin, G.X. Adaptive Self-Assembly and Induced-Fit interconversions between molecular borromean rings, russian dolls and Ring-in-Ring complexes. *Chin. J. Chem.* **2021**, *39*, 360–366. [[CrossRef](#)]
32. Liu, G.; Liu, X.-Q.; Sun, L.-B. Recent Advances in Metal-Organic Cages-Based Composite Membranes. *Chin. J. Struct. Chem.* **2022**, *41*, 2211100–2211109.
33. Zhang, H.N.; Yu, W.B.; Lin, Y.J.; Jin, G.X. Stimuli-Responsive topological transformation of a molecular borromean ring via controlled oxidation of thioether moieties. *Angew. Chem. Int. Ed.* **2021**, *60*, 15466–15471. [[CrossRef](#)]
34. Bai, S.; Han, Y.-F. Metal-N-Heterocyclic Carbene Chemistry Directed toward Metallosupramolecular Synthesis and Beyond. *Acc. Chem. Res.* **2023**, *56*, 1213–1227. [[CrossRef](#)]
35. Li, Y.; Yu, J.-G.; Ma, L.-L.; Li, M.; An, Y.-Y.; Han, Y.-F. Strategies for the construction of supramolecular assemblies from poly-NHC ligand precursors. *Sci. China. Chem.* **2021**, *64*, 701–718. [[CrossRef](#)]
36. Zhang, Y.-W.; Bai, S.; Wang, Y.-Y.; Han, Y.-F. A strategy for the construction of triply interlocked organometallic cages by rational design of poly-NHC Precursors. *J. Am. Chem. Soc.* **2020**, *142*, 13614–13621. [[CrossRef](#)]
37. Chen, T.; Zhao, Y.; Dang, L.-L.; Zhang, T.-T.; Lu, X.-L.; Chai, Y.-H.; Aznarez, F.; Ma, L.-F. Self-Assembly and Photothermal Conversion of MetallaRussian Doll and Metalla[2]catenanes Induced via Multiple Stacking Interactions. *J. Am. Chem. Soc.* **2023**, *145*, 18036–18047. [[CrossRef](#)]
38. Li, G.F.; Zhou, Z.X.; Yuan, C.; Guo, Z.W.; Liu, Y.H.; Zhao, D.; Liu, K.; Zhao, J.; Tan, H.W.; Yan, X.Z. Trackable Supramolecular Fusion: Cage to Cage Transformation of Tetraphenylethylene-Based Metallo-assemblies. *Angew. Chem. Int. Ed.* **2020**, *59*, 10013–10017. [[CrossRef](#)]
39. Mu, C.Q.; Zhang, Z.Y.; Hou, Y.L.; Liu, H.F.; Ma, L.Z.; Li, X.P.; Ling, S.L.; He, G.; Zhang, M.M. Tetraphenylethylene-Based Multicomponent Emissive Metallacages as Solid-State Fluorescent Materials. *Angew. Chem. Int. Ed.* **2021**, *60*, 12293–12297. [[CrossRef](#)]
40. Zhang, H.-N.; Feng, H.-J.; Lin, Y.-J.; Jin, G.-X. Cation-Templated Assembly of 6₁³ and 6₂³ Metalla-Links. *J. Am. Chem. Soc.* **2023**, *145*, 4746–4756. [[CrossRef](#)]
41. Yang, Y.; Ronson, T.K.; Lu, Z.; Zheng, J.; Vanthuyne, N.; Martinez, A.; Nitschke, J.R. A curved host and second guest cooperatively inhibit the dynamic motion of corannulene. *Nat. Commun.* **2021**, *12*, 4079. [[CrossRef](#)]
42. Yang, X.G.; Zhang, J.R.; Tian, X.K.; Qin, J.H.; Zhang, X.Y.; Ma, L.F. Enhanced Activity of Enzyme Immobilized on Hydrophobic ZIF-8 Modified by Ni²⁺ Ions. *Angew. Chem. Int. Ed.* **2023**, *62*, e202216699. [[CrossRef](#)]
43. Zhang, Z.-E.; Zhang, Y.-F.; Zhang, Y.-Z.; Li, H.-L.; Sun, L.-Y.; Wang, L.-J.; Han, Y.-F. Construction and Hierarchical Self-Assembly of Multifunctional Coordination Cages with Triangular Metal-Metal-Bonded Units. *J. Am. Chem. Soc.* **2023**, *145*, 7446–7453. [[CrossRef](#)]
44. Guo, S.-T.; Cui, P.-F.; Liu, X.-R.; Jin, G.-X. Synthesis of Carborane-Backbone Metallacycles for Highly Selective Capture of *n*-Pentane. *J. Am. Chem. Soc.* **2022**, *144*, 22221–22228. [[CrossRef](#)]
45. Cui, P.-F.; Liu, X.-R.; Lin, Y.-J.; Li, Z.-H.; Jin, G.-X. Highly Selective Separation of Benzene and Cyclohexane in a Spatially Confined Carborane Metallacage. *J. Am. Chem. Soc.* **2022**, *144*, 6558–6565. [[CrossRef](#)]
46. Chen, R.; Chen, G.; He, Y.; Zhang, J. Coordination Assembly of Tetrahedral Ti₄(embonate)₆ Cages with Alkaline-Earth Metal Ions. *Chin. J. Struct. Chem.* **2022**, *41*, 2201001–2201006.

47. Guo, J.; Fan, Y.Z.; Lu, Y.L.; Zheng, S.P.; Su, C.Y. Visible-light photocatalysis of asymmetric [2+2] cycloaddition in cage-confined nanospace merging chirality with triplet-state photosensitization. *Angew. Chem. Int. Ed.* **2020**, *59*, 8661–8669. [[CrossRef](#)]
48. Cai, L.X.; Li, S.C.; Yan, D.N.; Zhou, L.P.; Guo, F.; Sun, Q.F. Water-Soluble Redox-Active Cage Hosting Polyoxometalates for Selective Desulfurization Catalysis. *J. Am. Chem. Soc.* **2018**, *140*, 4869–4876. [[CrossRef](#)]
49. Wang, L.-J.; Li, X.; Bai, S.; Wang, Y.-Y.; Han, Y.-F. Self-Assembly, Structural Transformation, and Guest-Binding Properties of Supramolecular Assemblies with Triangular Metal-Metal Bonded Units. *J. Am. Chem. Soc.* **2020**, *142*, 2524–2531. [[CrossRef](#)]
50. Wang, L.-J.; Bai, S.; Han, Y.-F. Water-Soluble Self-Assembled Cage with Triangular Metal–Metal-Bonded Units Enabling the Sequential Selective Separation of Alkanes and Isomeric Molecules. *J. Am. Chem. Soc.* **2022**, *144*, 16191–16198. [[CrossRef](#)]
51. Liu, T.; Bai, S.; Zhang, L.; Hahn, F.E.; Han, Y.-F. N-Heterocyclic Carbene-Stabilized Metal Nanoparticles within Porous Organic Cages for Catalytic Applications. *Natl. Sci. Rev.* **2022**, *9*, nwa067. [[CrossRef](#)]
52. Zhao, X.; Qiu, H.; Shao, Y.; Wang, P.; Yu, S.; Li, H.; Zhou, Y.; Zhou, Z.; Ma, L.; Tan, C. Silver nanoparticle-modified 2D MOF nanosheets for photothermally enhanced silver ion release antibacterial treatment. *Acta Phys. Chim. Sin.* **2023**, *39*, 2211043. [[CrossRef](#)]
53. Liu, J.-C.; Wang, J.-F.; Han, Q.; Shanguan, P.; Liu, L.-L.; Chen, L.-J.; Zhao, J.-W.; Streb, C.; Song, Y.-F. Multicomponent Self-Assembly of a Giant Heterometallic Polyoxotungstate Supercluster with Antitumor Activity. *Angew. Chem. Int. Ed.* **2021**, *60*, 11153–11157. [[CrossRef](#)]
54. Lu, H.-L.; Tong, J.; Ma, H.-W.; Yu, S.-Y. Iodine Adsorption Studies of Dipalladium-based Supramolecular Cages. *Chin. J. Struct. Chem.* **2021**, *40*, 1680–1686.

Disclaimer/Publisher’s Note: The statements, opinions and data contained in all publications are solely those of the individual author(s) and contributor(s) and not of MDPI and/or the editor(s). MDPI and/or the editor(s) disclaim responsibility for any injury to people or property resulting from any ideas, methods, instructions or products referred to in the content.